Bilge International Journal of Science and Technology Research

ISSN: 2651-401X
e-ISSN: 2651-4028
Research Article

2022, Volume: 6, Issue: 1, 52-61
Received: 28.02.2021; Accepted: 23.03.2021
DOI: 10.30516/bilgesci.1055529

Mineral Exploration and Lithological Mapping Using Remote Sensing Approaches In Between Yazıhan-Hekimhan (Malatya) Turkey

Yusuf Topak[1], Mamadou Traore[2*], Ulaş İnan Sevimli[1], Senem Tekin[1*]

Abstract: The Remote Sensing processing analysis has become a directing and hopeful instrument for mineral Exploration and lithological mapping. Mineral exploration in general and bearing chromites associated with ultrabasic and basic rocks of the ophiolite complex in particular has been successfully carried out in recent years using Remote Sensing techniques. Yazıhan-Hekimhan (Malatya) region of the East Taurus mountain belt, ranks second in terms of iron mineralization in Turkey are accepted. The area is characterized by high grade iron ore deposits in use, development and exploration. Lithological mapping and chromite ore exploration of this area is challenging owing to difficult access (High Mountain 2243 m) using the traditional method of exploration. The main objective of this research is to evaluate the capacity of Landsat-8 OLI and Advanced Spaceborne Thermal Emission and Reflection Radiometer (ASTER) satellite imagery to discriminate and detect the potential zone of chromites bearing mineralized in Malatya (Yazıhan). Several images processing techniques, Vegetation Mask, Band Ratio (BR), Band Ratio Color Composite (BRCC), Principal Component Analysis (PCA), Decorrelation Stretch, Minimum Noise Fraction and Supervised classification using Spectral Angle Mapper (SAM) exist in previous studies have been performed for lithological mapping. The obtained results show that BR, PCA and Decorrelation Stretch methods applied on NVIR-SWIR bands of Landsat-8 and ASTER were clearly discriminate the ophiolite rocks at a regional scale. In Addition, SAM classification was applied on a spectral signature of different ultrabasic and basic rocks extracted from ASTER data. The results are promising in identifying the potential zones of chromite ore mineralization zones within the ophiolite region. Thus, the techniques used in this research are suitable to detect or identify the high-potential chromite bearing areas in the ophiolite complex rocks using Landsat-8 OLI and ASTER data.

Keywords: Remote Sensing, Yazıhan - Hekimhan (Malatya) region, iron ore deposits, Vegetation Mask, Band Ratio Color Composite, Principal Component Analysis.

[1]Address: Adıyaman University, School of Technical Sciences, TR-02040, Adıyaman, Turkey.

[2]Address: Bangui University, Faculty of Sciences, Departmen of Earth Sciences, Bangui, Central African Republic.

***Corresponding author**: senemtekin@adiyaman.edu.tr

Citation: Toprak, Y., Traore, M., Sevimli, U, İ., Tekin, S. (2021). Mineral Exploration and Lithological Mapping Using Remote Sensing Approaches In Between Yazıhan-Hekimhan (Malatya) Turkey. Bilge International Journal of Science and Technology Research, 6(1): 52-61.

1. INTRODUCTION

Recently, remote sensing is among the most powerful tools in geological research and mineral mapping (Rowan et al., 2006; Rajendran 2011; Pour et al. 2014 Zoheir et al., 2018; Noori et al., 2019; Pour et al., 2019a; Sekandari et al., 2020; Cardoso-Fernandes et al., 2020). However, it is possible to distinguish many alteration minerals and map them with more accuracy to understand the difference Furthermore, the development of new remote sensing methods, a few image processing methods have been discovered to map geological formations and they are also used in minerals research (Zhang et al., 2007; Hassan and Ramadan, 2015). Mineral exploration and geological mapping using remote sensing have been made effectively in arid, semi-arid and in other regions with little or high vegetation cover (Hellman and

Ramsey 2004; Pour et al., 2018a,b; Sheikhrahimi et al., 2019). several researchers have used spectral signatures (Rowan et al., 2006; Pour and Hashim, 2012; Pour et al., 2018b) for lithological mapping and mineral exploration based on remote sensing techniques. Minerals such as iron, hydroxyl, sulphate, dolomite, clay and carbonate have spectral characteristics in the Visible and Near-Infrared (VNIR) and Shortwave-Infrared (SWIR) domains, for the electromagnetic spectrum, whereas silicate minerals exhibit a spectral characteristic in the Thermal Infrared (TIR) region (Nimoyima 2005; Rowan et al., 2006).

Hydrothermal mineral mapping; which are most common indicators of mineralization is basic to reconnaissance and play an essential role in mineral exploration (Abdelsalam et al., 2000; Crósta et al. 2003; Loughlin 1991; Gabr et al. 2010; Kusky and Ramadan, 2002; Zhang et al., 2007; Madani, 2009; Gabr et al., 2015; Pour et al. 2018c, 2019a, b; Bolouki et al., 2020). The mineral assemblage found in the host rocks by Abrams et al. (1983) contained at least one mineral with diagnostic spectral absorption characteristics according to their study. Lithology describes the physical characteristics of rock units visible in the field, such as color, texture, grain size or composition. Lithological maps include the spatial distribution of rock units on the surface. Digital database produced from surface lithology provides support for the determination of land features such as geological mapping, mineral exploration and environmental characterization (Laake and Insley 2007; Laake, 2011, Rajendran et al., 2017, Özkan et al., 2017; Traore et al., 2020 a, b). Satellite images provide advantages in interpreting lithology the surface and near-surface structures (Laake and Insley 2007; Laake, 2011).

This study uses Aster and Landsat images of 174-033 rows and columns . The most important advantages of these images are that the images of the satellites are provided free of charge, they offer multi-band images to the users, they are suitable for medium-scale geological map production in spatial resolution, and they allow studies that cover large areas. This study aimed to investigate the use of geometric and radiometric corrected images in defining rock types and making maps for different lithological units within the scope of this study. In this context; Vegetation Mask, Band Ratio (BR), Band Ratio Color Composite (BRCC), Principal Component Analysis (PCA) analysis has been made in an area of approximately 1415 km^2 between Yazıhan and Hekimhan districts of Malatya province (Fig. 1).

Figure 1. Map of Malatya located in the Turkey.

2.GEOLOGICAL SETTING

According to the study and examined in the chapter, two different second rows of transgressive stages can be mentioned. First state; In the late Maastrichtian, with the emplacement of the Hocalıkova ophiolite in the region, the encrustation increased, the advancing region increased and some parts of the marine basin turned into land. In this phase, a basin was opened behind the Yuksekova- Baskil arc (ensialic) in the Late Campanian due to the effect of the stress forces; this basin matured in the Late Maastrichtian period and the basin closed in the Middle Eocene, and became terrestrial in the Upper Eocene period.) the first transgressive phase has been the most beautiful. Towards the end of the closure phase of the basin, during the Oligocene period, the region has completely transformed into a terrestrial environment and includes pebbles of Stork volcanics at its base. At the end of the Oligocene, the second period transgressive phase started and the region became the place where lake environments are located in the region. The impact of the Malatya Fault has been observed on young sediments. Soft-deformation structures were developed in the Late Miocene and Pliocene units. Depressions and uplift areas of the Malatya Fault have developed due to transtensional and transpressional movements. Volcanic rocks outcropping around Yazihan (Malatya) are represented by basalt and basalts with olivine. Volcanics show microlithic, flow, hypocrystalline porphyritic and texture, and geochemically alkaline and subalkali. In the rare earth element (REE) diagram of volcanic rocks normalized to the primary mantle, it is seen that they present a significant enrichment of light rare earth elements (LREE). In the spider diagram normalized to the primary mantle, they present enrichment with lithophile elements (LILE) with coarse cations such as Rb, Ba and K and consumption in terms of high valence cations (HFS). In the tectonomagmatic environment separation diagrams based on trace elements stable against alteration, it is seen that volcanic rocks fall in the direction of intracontinental basalt (Fig. 2).

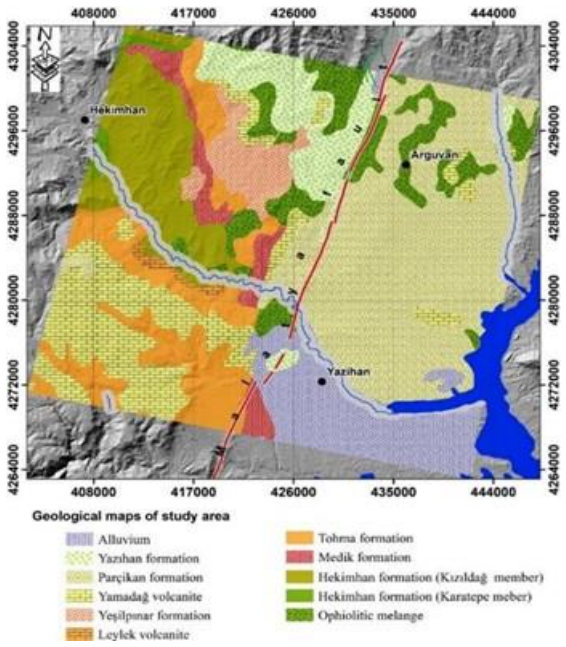

Figure 2. lithology map of the study area (Akbaş et al., 2002; Sevimli, 2009)

3.MATERIAL AND METHOD

3.1. Material and Preprocessing

Used in this study Visible near infrared and short-INFRAROUGE (VNR-SWIR) bands of Landsat-8 OLI and ASTER (Fig.3) the satellite satellite image of the US Geological Service (USGS) it is available as made of geometric and radiometric correction from the website. This image is in the Universal Transverse Mercator (UTM) coordinate system zone 37 and WGS84 datum. Satellite images processing, interpretation and data visualization processes, while field studies include controlling lithological units and contact boundaries detected by satellite images in the field. The contact relations, structural and textural properties of rocks belonging to different lithologies includes the comparison of the results obtained with the geological map and satellite images. The Aster image plays an important role in lithological discrimination. Table 4 gives a clear idea of the use of the Aster bands to explore mineral substances. The ASTER image was acquired in August 2001 during the dry period, with minimal green vegetation coverage These images correspond to images corrected radiometrically and geometrically. ASTER is composed of 14 strategically distributed spectral bands. The spatial resolution varies according to the wavelength, 15 m in the VNIR region (3 bands), 30 m in the SWIR region (6 bands), and 90 m for the three bands in the TIR region (Abrams and Hook, 2002) (Fig. 4).

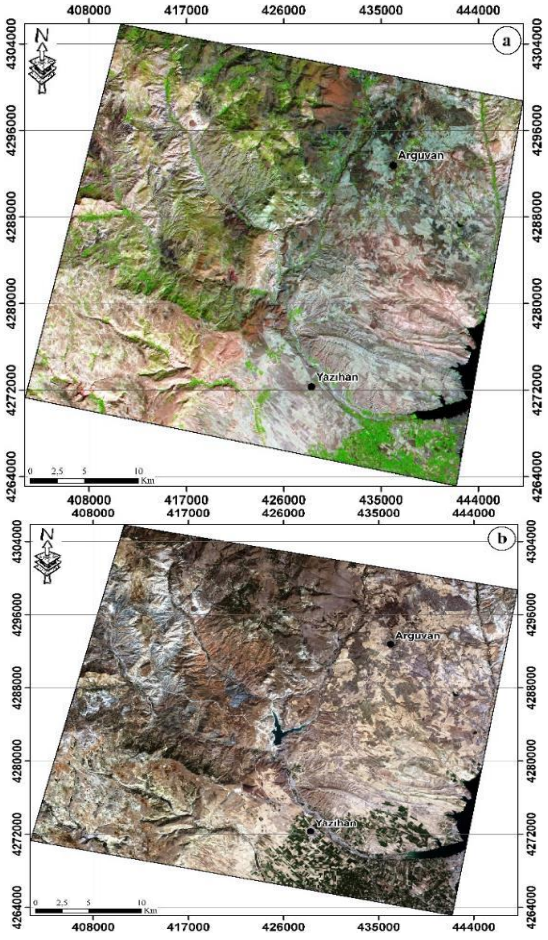

Figure 3. Aster (a) and Landsat-8 OLI (b) data of the study area.

Cross-talk correction does not apply in this research because the ASTER L1T SWIR bands had already been processed this correction. The atmospheric correction using Fast Line-of-sight Atmospheric Analysis of Spectral Hypercubes (FLAASH) algorithm was performed Aster image's VNIR and SWIR bands.

The variance of water vapor associated with different climate models is an important problem for the same bands of satellite data such as band 8 and band 9 of SWIR-ASTER image (Hewson, et al., 2005). Atmospheric correction reduces the influence of these factors (Moore et al., 2008, Pour et al., 2014).

This correction process requires the luminance image and therefore generates a reflectance corrected image. These effects were compensated for using the FLAASH tool of the ENVI software which uses the radiative transfer model M0DTRAN4.

.

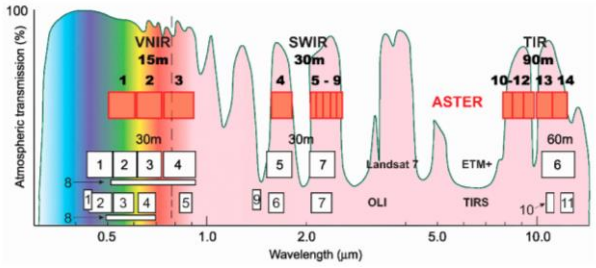

Figure 4. The spectral range and spatial resolution comparison for Landsat-8 (OLI), Landsat 7 (ETM +) and ASTER from USGS documents.

3.2. Methods

3.2.1. Band Raion Color Composite (BRCC)

Band rationing is an image enhancement analysis method in which new pixel values are obtained by dividing the gray color value of a pixel in one band by the value of the same pixel in another band or by applying other mathematical operations (Khan et al., 2007). In addition, by using this image enhancement method, the spectral differences between the bands are enriched and the effect of the terrain roughness on the images is reduced (Gupta et al.2005). The enriched images obtained from band proportions may not give the same results and interpretability in different geological and mineralogical environments and different topographies (Van der Wielen et al., 2004). Therefore, for this study, RGB (Red-Green-Blue) color composites of enriched bands obtained as a result of band proportioning applied to Landsat-8 OLI and ASTER bands were used to separate rock groups from each other and provide areal data. The steps of the working method are presented in Fig. 5.

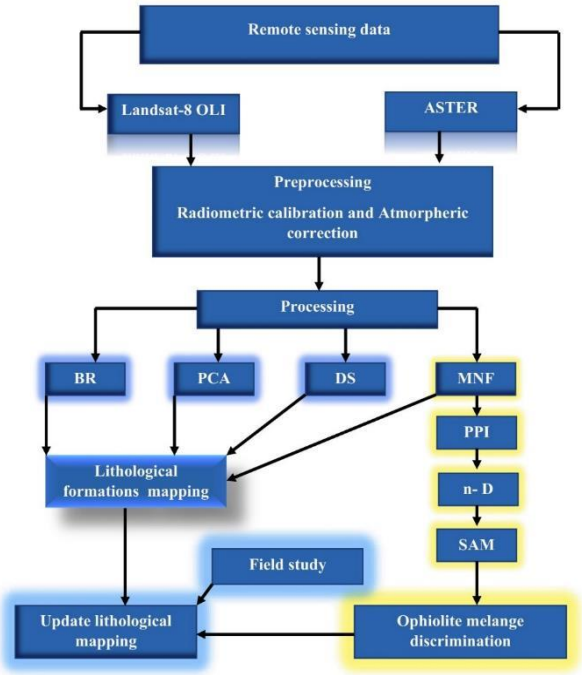

Figure 5. flowchart in this study.

3.2.2. Principal component analysis (PCA)

The principal component analysis is an effective technique for emphasizing a multispectral image for geological interpretation. Principal Component Analysis (PCA) is a mathematical processing method that minimizes information redundancy on different bands by translations and rotations. New axes are thus obtained and the different bands are "decorrelated" in the new reference marks established along these axes. The spatial resolutions of the different bands having been previously homogenized. The PCA was applied on nine bands of ASTER and Sven bands of Landsat-8 OLI in order to discriminate the lithological formations in this research.

3.2.3. Decorrelated stretching

Decorrelated stretching is a method used to interpret thermal infrared spectral data and enhances emissivity values between bands (Hook, et al., 2005). In this same procedure the effects of fringes between images are also eliminated (Guillespi, et al, 1987). Decorrelated stretching was used to determine the distribution of lithologies based on the increase in variations between spectral signature of bands related to differents lithogical formation and particullary in ophiolite melange rocks of the study area.

3.2.4. Supervised Classification

The following procedure replaces the methodology for using pure spectral signatures from fieldwork. This procedure includes extracting pure spectral signatures from ASTER bands in order to obtain a reference for ophiolite rocks of the study area. The first step was to calculate an Minimum Noise Fraction (MNF) on the emissivity bands to reduce noise. MNF is a transformation used to determine the inherent dimensionality of spectral data and to isolate noise (Boardman and Kruse, 1994). The second step was to establish the PPI purity index from the results of the MNF in order to isolate the pure members, and their respective spectral signatures were performed using Spectral Angle Mapper (SVM).

The SAM supervised classification method was applied in this study to map the lithology formations. SAM determines the similarity between a reference (r) and the unknown spectrum of the pixel (t) by calculating the vector angle (a) between the two in n-dimensions (Kruse, et al, 1993). SAM made it possible to determine the similarity between the spectral signature of emissivity of the lithologies extracted by the PPI purity index (reference spectrum) and the pixels of the rest of the image (unknown spectra) from the calculation of the angles between the 2 vectors.

4. RESULTS AND DISCUSSION

4.1. Vegetation Mask

The presence of vegetation and water masks a significant percentage of our study area although we have an acquisition date where water and vegetation are at their weakest cover. To eliminate the vegetation, we produced a mask from using Normalized Difference Vegetation Index (NDVI) and using the ratio of High reflectance (NIR) and high absorption (Red) spectrum carhacterized by the bands 4 and 5 for Landsat-8 OLI, and bands 2 and 3 for ASTER image equation 1. However, To mask the water body, the Normalized Difference Water Index (NDWI). This index uses the near infrared (NIR) and the Short-Wave infrared (SWIR) bands correspond to the bands 5 and 6 for Landsat-8 OLI , and bands 3 and 4 for ASTER image. NDWI can be calculated by following equation 2. Figure 5 shows the water and vegetation masks obtained.

NDVI = (NIR – Red) / (NIR + Red)
NDWI = (NIR – SWIR) / (NIR + SWIR)

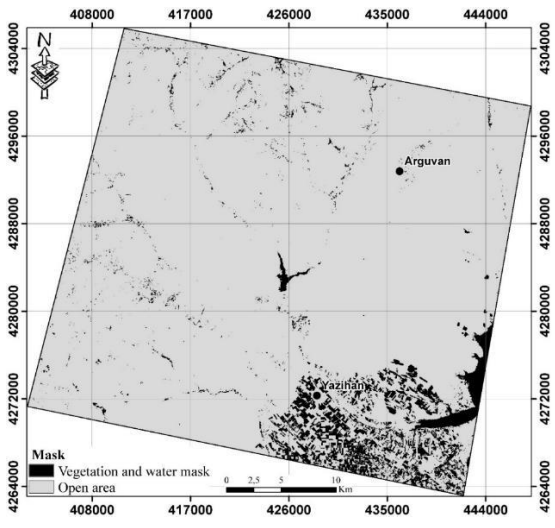

Figure 6. Vegetation and water mask in the study area.

4.2. BRCC

Previous studies have shown the ability of Landsat and ASTER VNIR-SWIR bands to map lithology formations and ophiolitic complexes (Amer et al., 2010; Rajendran et al., 2011; Ramadan 2013; Özkan et al., 2017; Traore et al.,

2020a). Based on the characteristics of the spectral bands of Landsat-8 OLI and ASTER image data, specialized band ratios of (7/4, 6/3, 5/7) and (7/6, 6/5 and 4/2) in RGB (Red, Green and blue) of the Landsat-8 OLI satellite image, and ((2 + 4) / 3, (5 + 7) / 6, (7 + 9) / 8), and a new band ratio (3/5, 4/6, 7/6) in RGB from ASTER image acquired in the dry season, and after different corrections applied in these data, allowed the map the geological formation and distinguished especially the ophiolite rocks of the study area. Its notes that the boundaries of the ophiolitic complexes have been clearly distinguished using these colored BRCC (Fig. 7).

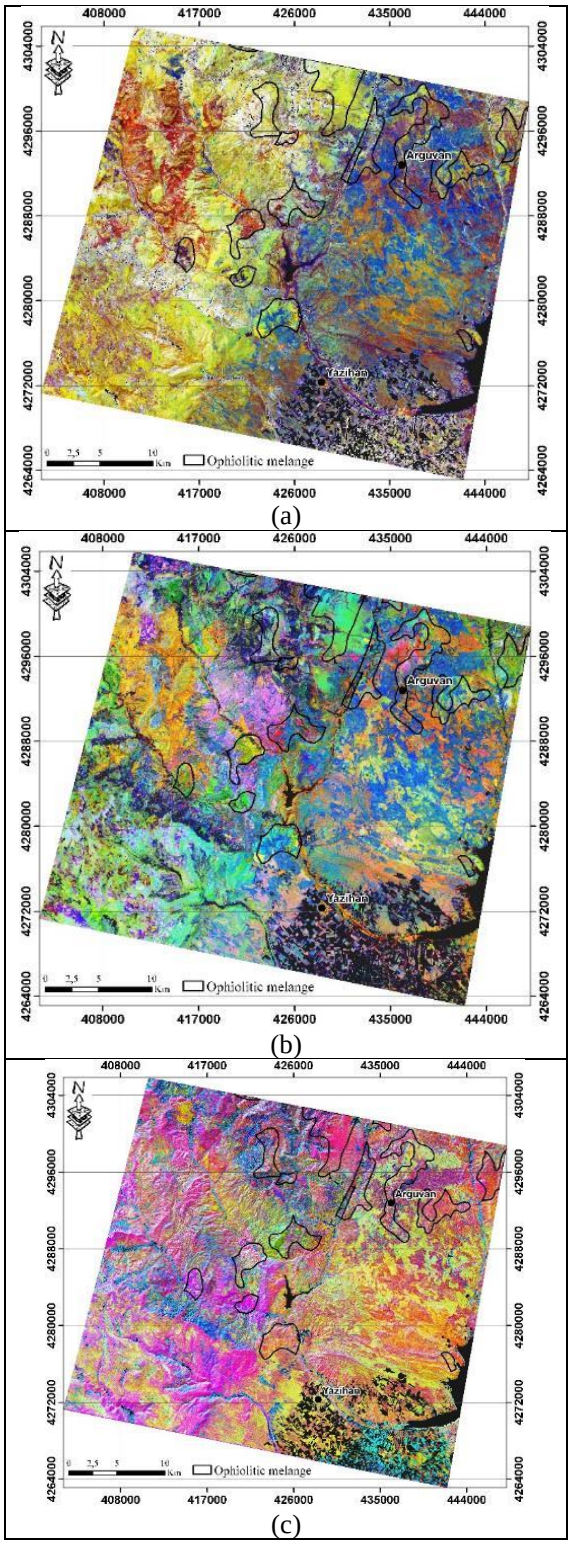

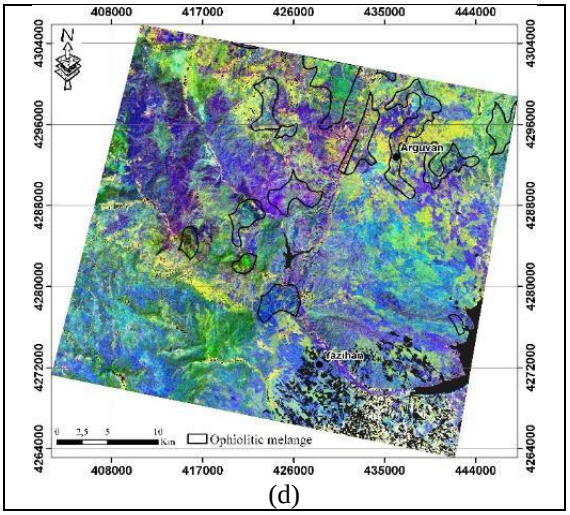

Figure 7. Band ratio (a) (7/4, 6/3, 5/7) and (b) (7/6, 6/5 and 4/2) in RGB from The Landsat-8 OLI, and (c) ((2 + 4) / 3, (5 + 7) / 6, (7 + 9) / 8) and (d) new 3/5 4/ 6 7/6 in RGB from ASTER image.

4.3.PCA

In order to differentiate the ophiolitic complex from other lithological formations in our study area, we used the PCA analysis technique. This technique has been used successfully in recent years by several researchers for the exploration of weathering minerals but especially for the mapping of geological formations (Crosta, et al., 2003, Pour et al., 2014, Rajendran et al., 2017, Özkan et al., 2017, Traore et al., 2020 a, b). The visible and near infrared bands of Landsat-8 OlI and ASTER data were selected and a PCA analysis was applied. The statistics related to the loading of each of the bands for each of the components (eigenvectors) were analyzed. The results allowed us to make a good lithological discrimination between the formations in our study region. Consequently, the band (PC1, PC2, PC3) and (PC1, PC3, PC5) in RGB for Landsat-8 OLI, and the band (PC1, PC5, PC6) and (PC4, PC2, PC1) in RGB for ASTER data were selected for good discrimination of ophiolites rocks among the other lithological formation in the study area (Figure 8). The results of visual image interpretation show that, the high ophiolites rocks are discriminated by yellow color in (PC1, PC2, PC3) and light pink-yellow color in (PC1, PC3, PC5) from Lansat-8 OLI (Fig. 8 a, b). According to the result from ASTER, the potential ophiolites rocks are distinguished by pink and yellow color in (PC1, PC5, PC6), and orange-yellow and light green-yellow color in (PC4, PC2, PC1) (Fig. 8 c,d).

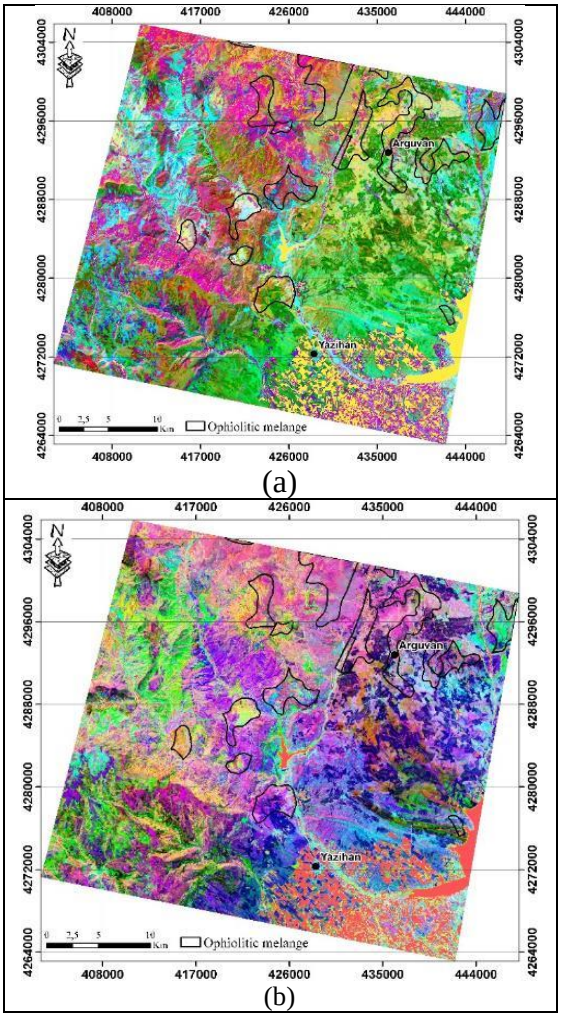

Figure 8. RGB color composites of (a) PCA (1, 2,3), (b) PCA (1, 3, 5) extracted from Landsat-8 OLI image, and RGB color composites of (c) PCA (1, 5,6) and (d) PCA (4, 2, 1) from ASTER data of the study area.

4.4. Decorrelation stretching

Recently, decorrelated stretching is one of the most important methods used in remote sensing research to map the lithology formations. Usually, the data from the spectral VNIR and SWIR bands are used and analyses the effect of enhancing the emissivity values between the bands (Hook, et al., 2005). In this same procedure, the impact of fringes between images are also eliminated (Guillespi et al, 1987). In this study, decorrelated stretching was used only from VNIR-SWIR bands of Landsat-8 OLI to map the distribution of lithological rocks. Based on the spectral signature of rocks in the study area, the (2, 4, 6) and (7, 6, 5) bands were selected (Hubbard et al., 2007; Rajendran et al., 2011). The results of this method are presented in figure 9. to better appreciate the results and distinguish the ophiolite rocks from other lithology formations, the spatial observation of the results obtained was superimposed on the contour of the ophiolitic complexes of the reference geological mapping of our area. The dark blue and red colored areas correspond to ophiolitic rocks when using bands (2, 4 and 6) in RGB. On the other hand, these same formations appear in light green and yellow color in the bands (7, 6, 5) in RGB (Fig. 9).

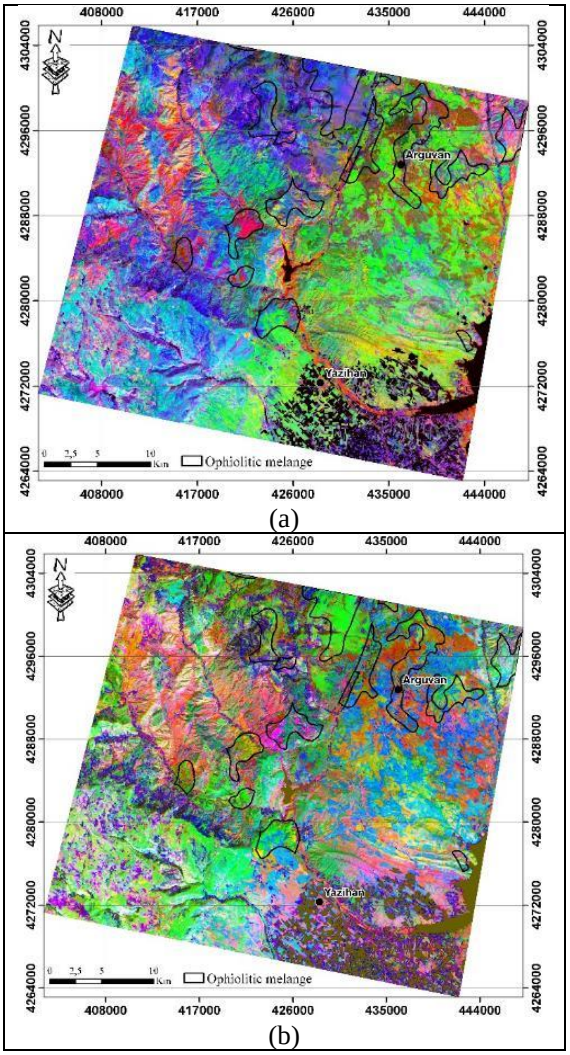

Figure 9. Landsat-8 OLI RGB (a) (2, 4, 6) and (b) (7, 6, 5) bands decorrelated image of study area.

4.5. Minimum Noise Fraction (MNF)

The ability to map rocks using multispectral satellite data is enhanced by the different bands, which are sensitive to differences in rock mineralogy. The calculation of MNF is likely to provide the maximum lithological information. The importance to use the MNF technique is to distinguish all possible color combinations of Landsat-8 OLI and ASTER data bands for lithological mapping. The MNF technique was applied to VNIR-SWIR Landsat-8 OLI and ASTER bands. Table 1 shows the statistical results for MNF components of the seven bands of Landsat-8 OLI and nine band of ASTER SWIR bands. The MNF shown in RGB allowed us to distinguish the colors that correspond to the different rocks in our study area (figure 10). The result of band 1,2 and 3, and 4,3 and 2 in RGB of Landsat-8 OLI showed that ophiolite melange rocks appear as a melange of color characterized by green to yellow and dark blue color in North of the study area (Fig. 10 a,b). However, the result of band 1, 2 and 3, and 4,2 and 3 in RGB of ASTER data showed that ophiolite complexes rock manifest as dark pink and light-yellow color in this research (Fig. 10 c,d).

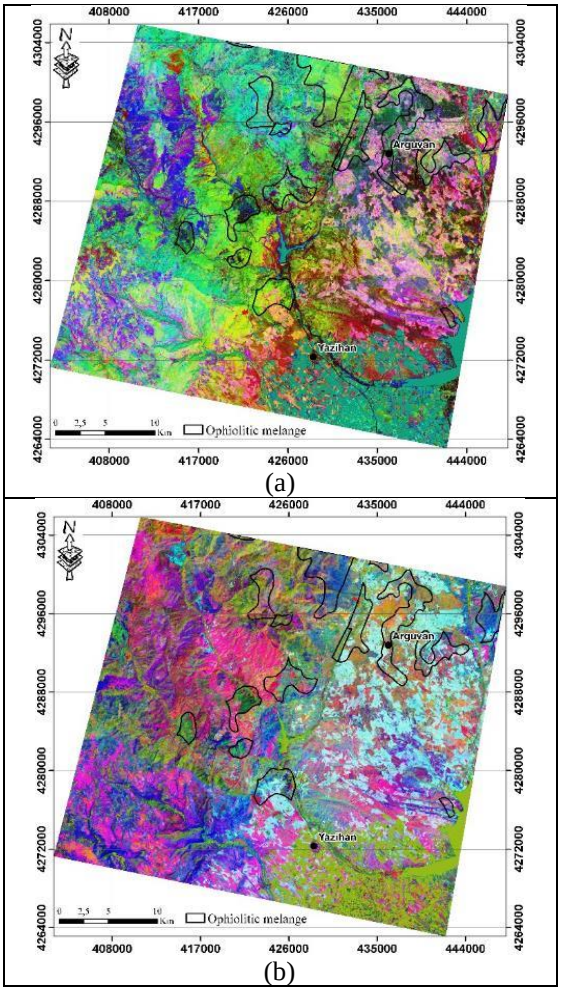

Figure 10. RGB color composites of (a) MNF (1, 2,3), (b) MNF (4, 2, 1) extracted from Landsat-8 OLI image, and RGB color composites of (c) MNF (1, 2,3) and (d) MNF (4, 3, 2) from ASTER data.

4.6.Supervised classification

MNF is a transformation used to determine spectral data's inherent dimensionality and isolate noise (Boardman and Kruse, 1994). The second step was to establish the PPI purity index from the results of the MNF to isolate the pure members, the Identification of Endmembers was applied, their respective spectral signatures of ophilites complex rocks (Fig.11b) were selected and finally, themap distribution and abundance were performed using Spectral Angle Mapper (SVM) (Fig.11 a).

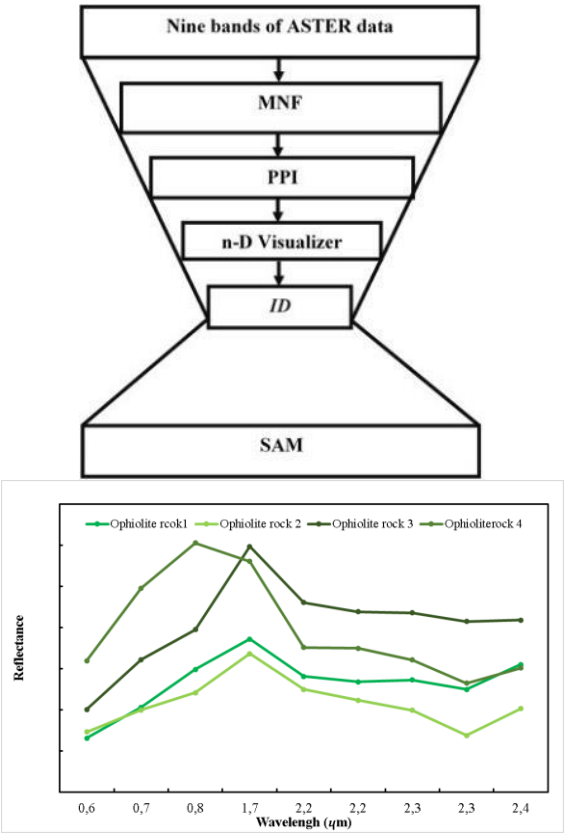

Figure 11. (a) Standardized ASTER analysis scheme for ophiolite mapping using the spectral hourglass approach and (b) the selected n-D classes (end-member spectra) extracted from ASTER data of ophiolite melange rock.

The analysis of the results of Decorrelation stretching (DS) and PCA allows us to makes the interpretations and comparation of map ophiolite melange rock with the available geological of study area. The result of DS such as (7, 6, 5) (Fig. 12a) display to the RGB color showed Ophiolite melange rocks were clearly in light to maroon color. However, the ophiolites melange rocks were also differentiatedin light green-yellow color using PCA (4, 2, 1) in RGB (Fig. 12 b). Based on the result of DS and PCA bands, It is important to note.

The result of this classification is illustrated in figure 12 c. The reference vector is constructed to perform the SAM classification.The angle between the reference vector and the pixel vector is calculated to compare with the determined threshold angle value. In total, the pure spectral signatures were determined to correspond to the lithologhy of the ophiolitic complex rocks. These signatures were compared to the USGS spectral library to associate a lithology name with the calculated signature. The ophiolitic rocks were mapped with the SAM method using the references obtained from the previous step. A visual representation of the SAM results is shown in Figure 12c where these rocks have been identified in green color. The comparison of the result of this classification with an old delineation of the ophiolitic rocks of our study area, showed an excellent correspondence.

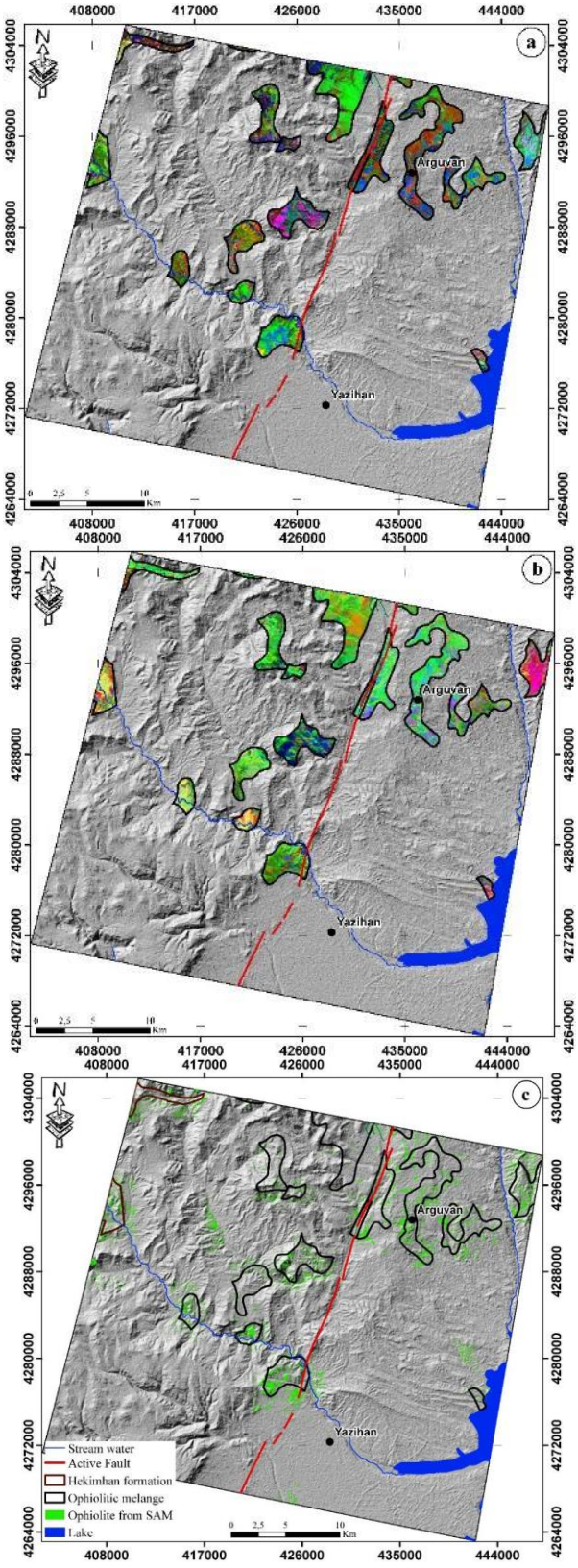

Figure 12. Ophiolite melange zone extracted from (a) Decorrrelated stretch (7, 6, 5), (b) PCA (4, 2, 1) in RGB and Ophiolite mapping using SAM in the study area.

5. FIELD INVESTIGATION

The ophiolite unit, which crops out in large areas in the study area, consists of dunite, harzburgite, pyroxenite, gabbro and spilite. The images of the formations that are common in the region in the field studies carried out in the study area are shown in Figure 13. Most of the ultramaphic and mafic rocks are serpentinized in the ophiolite regions. Volcanites are generally of Spilitic type and red pelagic deposits are located in the uppermost levels of the ophiolite. Sediments; consists mainly of calcitic dolostone, radiolarite and mudstone. It is easily distinguished from other rocks of ophiolite with its red, brown and pink colors. (Fig. 13 a, b and c).

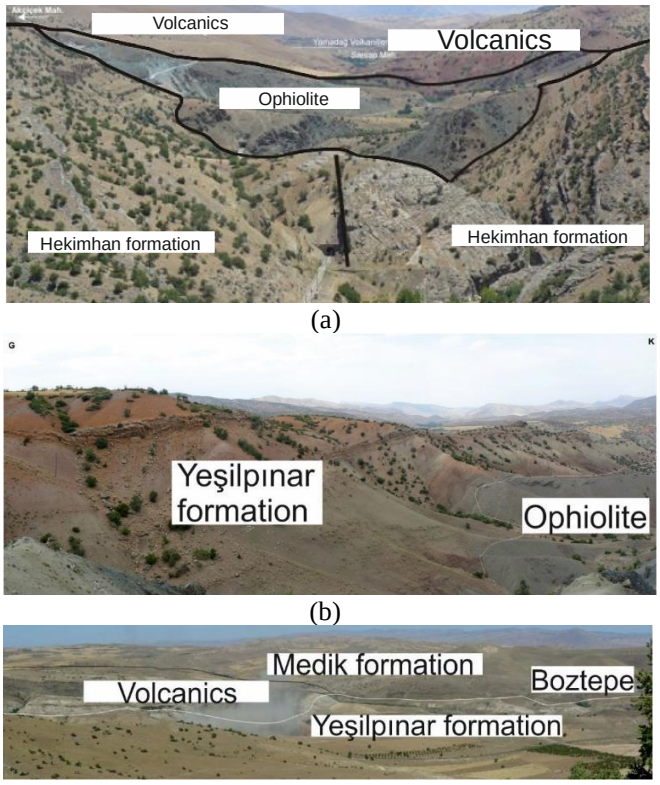

Figure 13. Field photographs of the study area.

6. CONCLUSION

The study illustrates the capability and how RS and GIS techniques can be used to correlate the previous lithological and mineral, between the integration multispectral data (ASTER, Landsat-8 OLI and ASTER, fieldwork, Geochemistry and Petrographic analysis. In this study, ASTER and Landsat-8 OLI satellite image data for Malatya were processed and tested for detected the potential zones for chromite bearing mineral and updating lithological map of the study area. The special distribution of ophiolite melange rocks were mapped using band combinations, BR, PCA, DS, MNF and SAM image processing techniques. The result indicates that, the different methods performed on spectral bands (VNIR-SWIR) of Landsat-8 OLI and ASTER data demonstrates successful in discrimination of ophiolite melange rocks and depiction of the zone of chromite ore bearing zone within ophiolites in this region. The results obtained from SAM showed high ability of this techniques for in ophiolite differentiations. It shows also a good virtual correlation with the previous geological map of the study area. The statistical results derived from virtual verification, the previous geological map and geological formations in the field shows that the overall accuracy and Kappa Coefficient 82.51% and 0.86 for SAM respectively. This research suggests that, the discrimination of ophiolitic complexes and exploration of potential of chromite ore deposits zone can be

performed using the processing techniques applied in this study.

Ethics Committee Approval
N/A

Peer-review
Externally peer-reviewed.

Author Contributions
Conceptualization, Investigation, Material and Methodology, Supervision, Visualization, Writing-Original Draft, Writing-review & Editing: İ.G. Other: The author has read and agreed to the published version of manuscript.

Conflict of Interest
The authors have no conflicts of interest to declare.

Funding
The authors declared that this study has received no financial support.

REFERENCE

Abdelsalam MG, Stern RJ, Berhane WG. (2000). Mapping gossans in arid regions with Landsat TM and SIR-C images: the Beddaho Alteration Zone in northern Eritrea. Journal of African Earth Sciences, 30(4), 903-916.

Abrams MJ, Brown D, Lepley L, Sadowski R. (1983). Remote sensing for porphyry copper deposits in southern Arizona. Economic Geology, 78(4), 591-604.

Akbaş B, Akdeniz N, Aksay A, Altun İ, Balcı V, Bilginer E, Bilgiç T, Duru M, Ercan T, Gedik İ, Günay Y, Güven İH, Hakyemez, HY, Konak N, Papak İ, Pehlivan Ş, Sevin M, Şenel M, Tarhan N., Turhan N, Türkecan A, Ulu Ü, Uğuz MF, Yurtsever A, (2002). Turkey Geology Map General Directorate of Mineral Reserach and Exploration Publications. Ankara Turkey.

Amer R, Kusky T, Ghulam A. (2010). Lithological mapping in the central eastern desert of Egypt using ASTER data. J. Afr. Earth Sci. 56, 75–82.

Boardman JW, Kruse FA, Green RO. (1995). Mapping target signatures via partial unmixing of AVIRIS data. In: Summaries, Proceedings of the 5th JPL Airborne Earth Science Workshop. JPL Publ, Pasadena, California (95-1, 1: 23–26), January 23–26.

Bolouki SM, Ramazi HR, Maghsoudi A, Beiranvand Pour A, Sohrabi G. (2020). A Remote Sensing-Based Application of Bayesian Networks for Epithermal Gold Potential Mapping in Ahar-Arasbaran Area, NW Iran. Remote Sensing, 12(1), 105.

Cardoso-Fernandes J, Teodoro AC, Lima A, Roda-Robles E. (2020). Semi-automatization of support vector machines to map lithium (Li) bearing pegmatites. Remote Sensing, 12(14), 2319.

Crosta AP, Filho CRS, Azevedo F, Brodie C. (2003). Targeting key alteration minerals in epithermal deposits in Patagonia, Argentina, using ASTER imagery and principal component analysis. Int. J. Remote. Sens. 24, 4233–4240.

Gabr, S, Ghulam, A, Kusky, T. (2010). Detecting areas of high-potential gold mineralizations using ASTER data. Ore Geol. Rev. 38, 59–69. Gad, S., Kusky, T.M., 2007. ASTER spectral ratioing for lithological mapping in the Arabian– Nubian shield, the NeoproterozoicWadi Kid area, Sinai, Egypt. Gondwana Res. 11 (3), 326–335.

Gad S, Kusky T. (2007) ASTER spectral ratioing for lithological mapping in the Arabian–Nubian shield, the Neoproterozoic Wadi Kid area, Sinai, Egypt. Gondwana Research, 11(3), 326-335.

Kruse FA, Lefkoff B, Dietz JB, (1993). Expert system-based mineral mapping in northern Death Valley, California/Nevada, using the airborne visible/infrared imaging spectrometer (AVIRIS). Rem. Sensing Environ. 44 (2), 309–336.

Gillespie AR, Kahle AB, Walker RE, (1987). Color enhancement of highly correlated images. II. Channel ratio and "chromaticity" transformation techniques. Remote Sensing of Environment, 22(3), 343-365.

Gupta RP, Haritashya UK, Singh, P. (2005). Mapping dry/wet snow cover in the Indian Himalayas using IRS multispectral imagery. Remote Sensing of Environment, 97(4), 458-469.

Gupta RP, (2003). Remote Sensing Geology. Springer-Verlag Berlin, Heidelberg, Germany.

Hassan SM, Ramadan TM. (2015). Mapping of the late Neoproterozoic Basement rocks and detection of the gold-bearing alteration zones at Abu Marawat-Semna area, Eastern Desert, Egypt using remote sensing data. Arabian Journal of Geosciences, 8(7), 4641-4656.

Hellman MJ, Ramsey MS. (2004). Analysis of hot springs and associated deposits in Yellowstone National Park using ASTER and AVIRIS remote sensing. Journal of Volcanology and Geothermal Research, 135(1-2), 195-219.

Hewson RD, Cudahy TJ, Mizuhiko S, Ueda K, Mauger AJ, (2005). Seamless geological map generation using ASTER in the Broken Hill-Curnamona province of Australia. Remote Sensing of Environment, 99(1-2), 159-172.

Van der Wielen S, Oliver S, Kalinowski A, (2004). Remote sensing and spectral investigations in the Western Succession, Mount Isa Inlier: Implications for exploration. In CRC Conference, Barossa Valley (pp. 1-3). Khan et al., 2007 S.D. Khan, K. Mahmood, J.F. Casey Mapping of Muslim Bagh ophiolite complex (Pakistan) using new remote sensing, and field data

Kruse, FA, Lefkoff, B, Dietz, JB. (1993). Expert system-based mineral mapping in northern death valley, California/Nevada, using the airborne visible/infrared imaging spectrometer (AVIRIS). Rem. Sensing Environ. 44 (2), 309–336.

Laake A, Cutts, A. (2007). The role of remote sensing data in near-surface seismic characterization. first break, 25(2).

Laake A. (2011). Integration of satellite Imagery, Geology and geophysical Data. Earth and Environmental Sciences, (INTECH Open Access Publisher), 467-492.

Loughlin WP. (1991). Principal components analysis for alteration mapping. Photogramm. Eng. Rem. Sens. 57, 1163–1169.

Madani, A. A. (2009). Utilization of Landsat ETM+ data for mapping gossans and iron rich zones exposed at Bahrah area, Western Arabian Shield, Saudi Arabia. Journal of King Abdulaziz University: Earth Sciences, 20, 25-49.

Ninomiya, Y. (2003). Advanced Remote Lithologic Mapping in Ophiolite Zone with ASTER Multispectral Thermal Infrared Data. In Proceedings of the IEEE International Geoscience and Remote Sensing Symposium, Toulouse, France, 21–25 July; Volume 3, pp. 1561–1563.

Noori, L., Pour, B.A., Askari, G., Taghipour, N., Pradhan, B., Lee, C.-W., Honarmand, M. (2019). Comparison of different algorithms to map hydrothermal alteration zones using ASTER remote sensing data for polymetallic vein-type ore exploration: toroud–chahshirin magmatic belt (TCMB), north Iran. Rem. Sens. 11, 495. https://doi. org/10.3390/rs11050495.

Özkan, M., Çelik, Ö. F., Özyavaş, A. (2018). Lithological discrimination of accretionary complex (Sivas, northern Turkey) using novel hybrid color composites and field Pour et al. 2018 a, b, 2018c, 2019a, b;

Pournamdari, M., Hashim, M., Pour, A.B., (2014b). Application of ASTER and Landsat TM data for geological mapping of Esfandagheh ophiolite complex, southern Iran. Resource Geology, 64, 233–246.

Pour, A.B., Hashim, M. (2012). The application of ASTER remote sensing data to porphyry copper and epithermal gold deposits. Ore Geol. Rev. 44, 1–9.

Rajendran, S., Hersi, O.S., Al-Harthy, A.R., Al-Wardi, M., Elghali, M., Al-Abri, A.H. (2011). Capability of Advanced Spaceborne Thermal Emission and Reflection Radiometer (ASTER) on discrimination of carbonates and associated rocks and mineral identification of eastern mountain region (Saih HatatWindow) of Sultanate of Oman. Carbonates Evaporites 26, 351 –364.

Rajendran, S., Nasir, S. (2017). Characterization of ASTER spectral bands for mapping of alteration zones of Volcanogenic Massive Sulphide (VMS) deposits. Submitted to the Ore Geology Review.

Kusky TM, Ramadan TM. (2002). Structural controls on Neoproterozoic mineralization in the South Eastern Desert, Egypt: an integrated field, Landsat TM, and SIR-C/X SAR approach. Journal of African Earth Sciences, 35(1), 107-121.

Rowan LC, Schmidt RG, Mars JC, (2006). Distribution of hydrothermally altered rocks in the Reko Diq, Pakistan mineralized area based on spectral analysis of ASTER data. Remote Sens Environ. 104:74–87.

Sekandari, M., Masoumi, I., Beiranvand Pour, A.M., Muslim A., Rahmani, O., Hashim, M., Aminpour, S.M. (2020). Application of Landsat-8, Sentinel-2, ASTER and WorldView-3 Spectral Imagery for Exploration of Carbonate-Hosted Pb-Zn Deposits in the Central Iranian Terrane (CIT). Remote Sensing, 12(8), 1239.

Sevimli U.İ. (2009). Yazıhan (Malatya) Batısının Tektono-Stratigrafisi, Çukurova Üniversitesi, Fen Bilimleri Enstitüsü, Jeoloji Mühendisliği Anabilim Dalı. 159 Sayfa, Adana, (In Turkish).

Sheikhrahimi A, Pour A.B., Pradhan B, Zoheir B. (2019). Mapping hydrothermal alteration zones and lineaments associated with orogenic gold mineralization using ASTER data: A case study from the Sanandaj-Sirjan Zone, Iran. Advances in Space Research, 63(10), 3315-3332.

Traore M, Wambo JDT, Ndepete CP, Tekin S, Pour AB, Muslim A.M. (2020a). Lithological and alteration mineral mapping for alluvial gold exploration in the south east of Birao area, Central African Republic using Landsat-8 Operational Land Imager (OLI) data. Journal of African Earth Sciences, 170, 103933.

Traore M, Çan T, Tekin S. (2020b). Discrimination of Iron Deposits Using Feature Oriented Principal Component Selection and Band Ratio Methods: Eastern Taurus /Turkey, International Journal of Environment and Geoinformatics (IJEGEO), 7(2): 147-156. DOI: 10.30897/ ijegeo.673143

USGS, (2016). United States Geological Survey (Using ENVI). http://www.USGS.gov

Zhang X, Panzer M, Duke N. (2007). Lithologic and mineral information extraction for gold exploration using ASTER data in the south Chocolate Mountains (California). J. Photogramm. Remote Sens. 62, 271–282.

Zoheir B, El-Wahed MA, Pour, A.B., Abdelnasser, A. (2019). Orogenic Gold in Transpression and Transtension Zones: Field and Remote Sensing Studies of the Barramiya–Mueilha Sector, Egypt. Remote Sens. 2019, 11, 2122; doi:10.3390/rs11182122.